Stochastic simulation of porosity and acoustic impedance conditioned to seismic data and well data from the Troll field

Alfhild Lien Eide
Department of Mathematical Sciences
Norwegian University of Science and Technology
aeide@stat.ntnu.no

September 25, 1997

Abstract

A North Sea data set has been used to test a stochastic model for porosity and acoustic impedance conditioned to well data and seismic data. The assumptions in the partly Gaussian prior model are compared to the actual data set. A correlation structure is suggested on the basis on well data. Simulations from the posterior distribution, honoring well data and seismic data, are shown and compared to the prior model and the input data.

1 Introduction

A stochastic model for porosity and acoustic impedance conditioned to seismic data and well data was presented in Eide, Ursin & Omre (1997). This model is summarized in Figure 1.

This document presents a case study where this model is applied to data from the Troll field in the North sea. The reader should refer to Eide et al. (1997) for the theoretical background. A short presentation of the Troll field data set is given below. The data set is provided by Norsk Hydro ASA.

Section 2 discusses the prior model. In Section 3 the likelihood model for the observations is presented and in Section 4 the results of simulations from the posterior distribution are presented.

1.1 The Troll field data set

The seismic section shown in Figure 2 is taken from the Troll field in the North Sea. The interesting region is a 50 ms window below horizon 1. The seismic section is a so-called "random line" from a 3D dataset, that is, a broken line that does not correspond to any of the lines from the seismic survey. There are two wells on (or very close to) this line.

The lithology of the region is clean sands, micaceaous sands and some thin calcites. The presence of calcites may lead to questions about the Gaussianity assumption underlying the model described in Eide et al. (1997). This will be discussed in Section 2.

1.2 Seismic data

A window of 50 ms below horizon 1 will be studied here. The bottom of this window corresponds approximately to the next seismic horizon. This 50 ms window is outlined in Figure 2. In Figure 3 this region is flattened relatively to horizon 1 and displayed in a rectangular box. The vertical sampling of the seismic data is 2 ms.

1.3 Well data

The two wells A and B are located on or near the seismic line studied here. Both wells are vertical.

The following data are available from well logs: Depth, velocity v, density ρ and porosity ϕ. The velocity is calibrated with check shots, that is, VSP, to compensate for the fact that the log velocities are measured at other frequencies than seismic velocity. Acoustic impedance Z is calculated from density and velocity, $Z = \rho v$. Reflection coefficients are calculated from the acoustic impedances. Using the depth and velocity measurements, the log data have been converted from depth to time, and are sampled at 1 ms intervals. The resulting well data from well A and B are shown in Figure 4 and 5 respectively. To get an impression of the data, some data above and below the region under study have been included here.

1.4 Matching seismic data and well data

Ideally, a synthetic seismic trace calculated from the reflection coefficients in the wells should match the seismic data at the wells. Convolution of a 40 Hz Ricker wavelet, Figure 6, and the reflection coefficients from well A gives the synthetic trace shown to the left in Figure 7. The observed seismic trace is shown next to the synthetic trace for comparison. The strong reflection above horizon 1 is visible both in the synthetic and observed trace. The correlation between the traces shown is 0.83, which is a good correlation in a real data set. The correlation is reduced to 0.40 when using only the 50 ms window between the horizontal lines. However, this is a short window compared to the length of the seismic wavelet, which is 40 ms.

Similarly synthetic and observed traces for well B are shown to the right in Figure 7. The well log from this well has been shifted 5 ms down to match the observed data better. Still, the correlation between the synthetic and the observed trace is low. Some of the mismatch may be due to depth/time conversion. The depth/time conversion will not be treated thoroughly here. The well data are compared to the nearest seismic trace, but there may also be a location problem since these measurements are not made at exactly the same location.

Figure 8 shows correlation between the synthetic seismic traces and all the observed traces. Ideally, the correlation is expected to be high in traces near the well and decreasing away from the wells. But this figure shows that there is low correlation between observed traces and the synthetic traces from the wells. Another conclusion supported by this figure is that the strong reflection just above horizon 1 contributes much to the correlation.

Figure 9 shows correlation between the synthetic traces and observed traces for vertical shifts between -15 and 15 ms and for the 5 closest observed traces on each side of the well. Well A has a high correlation with all its neighboring traces, and it is clear that it should not be shifted up or down since the highest correlation is at shift 0. Well B has lower correlation. The maximum correlation appears to be at shift -10 and at traces 138-142.

Finally, these correlations should be kept in mind when the seismic noise model, Section 3.2 is considered.

2 Prior model

The model in Eide et al. (1997) assumes that reflection coefficients follow a Gaussian distribution. The histograms in Figure 10, 11 and 12 show the distributions of porosity, acoustic impedance and reflection coefficients based on the well observations. These data are the same as shown in Figure 4 and 5. Porosity and acoustic impedance do not appear to follow a Gaussian distribution. A bimodal distribution might give a better fit. An explanation of the possible bi-modality might be sought in the lithology in the region under study, which consists of clean sands, micaceaous sands and some calcites. However, the histograms of the reflection coefficients seem to have a Gaussian shape. The normal probability plots in Figure 13 show that the reflection coefficients in the section studied here are close to Gaussian, except perhaps that the tails of the distribution are a bit more heavy. That is, large positive and negative reflection coefficients are over-represented in this sample, compared to a Gaussian distribution.

2.1 Porosity

The use of seismic data in reservoir characterization depends on correlations between seismic properties (e.g. acoustic impedance), and reservoir properties (e.g. porosity). The model presented in Eide et al. (1997) assumes a linear dependence between porosity and acoustic impedance, but no correlation between reflection coefficients and porosity. The cross plots in Figure 14 indicate a negative correlation between acoustic impedance and porosity in this data set, while reflection coefficients and porosity appear to be uncorrelated. Hence the model assumptions seem to be valid for these data.

In Eide et al. (1997), the porosity is modeled as the sum of a function $\mu_\Phi(z)$ of the acoustic impedance z and a Gaussian random field U_Φ. Figure 15 shows 51 samples of ϕ and z from each well, totally 102 samples from the region below horizon 1. The data indicate a linear dependence between acoustic impedance and porosity. Linear regression of porosity against acoustic impedance gives

$$\hat{\phi} = \hat{b}_1 - \hat{b}_2 z = 0.5430 - 4.5263 \cdot 10^{-5} z \tag{1}$$

which is used as an estimate of $\mu_\Phi(z)$. The standard deviation of the residuals is 0.0331, which is used as an estimate of the variance of U_Φ.

To estimate the correlation structure of U_Φ, the trend function μ_Φ was subtracted from the porosity well logs. The empirical correlation function of the residuals is shown in Figure 16. An exponential correlation function with range 4 and exponential order $\nu = 1.2$ is shown in the same figure. This correlation function gives a good fit up to about 20 ms vertical distance, which is approximately the half the length of the wavelet, see Figure 6. The seismic resolution is usually assumed to be approximately 1/4 wavelength, hence it is more important to have a good prior model for the correlation structure below seismic resolution.

2.2 Reflection coefficients and acoustic impedance

The reflection coefficient field is modeled as a Gaussian random field with zero mean and covariance function

$$\mathrm{Cov}[C(x',t'),C(x'',t'')] = \sigma^2\rho(x''-x',y''-y') \tag{2}$$

where σ^2 is the variance and $\rho(\cdot,\cdot)$ the spatial correlation function of C. The shape of the spatial correlation function is important for the appearance of the resulting reflection coefficient field. It is also important for the resulting acoustic impedance field, generated through the transformation (8) in Eide et al. (1997), as illustrated in Figure 1.

The empirical correlation function for the reflection coefficients, based on well data from both wells, is shown in Figure 17. The empirical correlation function resembles white noise, but from Figure 4 and 5 it seems that large positive reflection coefficients are followed by large negative reflection coefficients. This suggests that there should be some structure in the reflection coefficients, and in particular the correlation function should give negative correlation at short ranges.

The relationship to acoustic impedance may help in the selection of a correlation function for the reflection coefficients: Let $C_{i,j}$ and $Z_{i,j}$ denote reflection coefficient and acoustic impedance at (x_i,t_j) and assume $\mathrm{E}(Z)=\theta$ and $\mathrm{var}(Z)=\sigma_Z^2$. Then

$$C_{i,j} = \frac{Z_{i,j+1}-Z_{i,j}}{Z_{i,j+1}+Z_{i,j}} \approx \frac{1}{2\theta}(Z_{i,j+1}-Z_{i,j}) \tag{3}$$

To obtain a correlation function for C, the following approximation is used: Assume for a moment that both Z and C are Gaussian, and that the relationship between these variables is linear, as on the approximative right hand side of Equation (3). The covariance function of C can be then be approximated as

$$\begin{aligned}\mathrm{Cov}(C_{i,j},C_{k,l}) &\approx \frac{1}{4\theta^2}\mathrm{Cov}(Z_{i,j+1}-Z_{i,j},Z_{k,l+1}-Z_{k,l}) \\ &= \frac{\sigma_Z^2}{4\theta^2}[2\rho(Z_{i,j},Z_{k,l})-\rho(Z_{i,j+1},Z_{k,l})-\rho(Z_{i,j},Z_{k,l+1})]\end{aligned} \tag{4}$$

where $\rho(\cdot,\cdot)$ denotes the correlation function of the acoustic impedance.

An exponential correlation function

$$\rho(Z(x',t'),Z(x'',t'')) = \exp\left(-3\left(\frac{\|(x'',t'')-(x',t')\|}{a}\right)^{\nu}\right) \tag{5}$$

with range $a=15$ and $\nu=1.4$ was fitted to the empirical correlation function of acoustic impedance from well data shown in Figure 18. As for porosity, the important part to fit is up to the pulse length. The fitted correlation function gives a good fit up to about 40 ms, which is more than the length of the seismic wavelet. The negative correlation at larger distances may be due to facies layering.

Using $a = 15$ and $\nu = 1.4$ from the acoustic impedance correlation function, a correlation function for C is calculated from Equation (4). The covariance in Equation (4) contains the parameters σ_Z^2 and θ. These cancel from the normalization when the correlation function is calculated, hence there is no need to estimate these parameters. This correlation function is shown in Figure 17 together with the empirical correlation of C.

This estimation gives the vertical range of the correlation function. The correlation function (4) is anisotropic. In addition, one may use an anisotropic distance measure in (5) to give the reflection coefficients and acoustic impedance a longer range in the lateral direction. The well data do not give any information on the horizontal range of the correlations. If no other sources of information are available, the horizontal range of the correlation should be decided from expert judgments about the lateral continuity of the petrophysical and geophysical properties.

2.3 The "integration constant" z_0

The "integration constant" $z_0 = Z(x_i, t_0)$ is involved in the transformation from reflection coefficients to acoustic impedances, see Equation (8) in Eide et al. (1997). In the realizations from the prior model shown in Section 2.4, a constant z_0 is used. When simulating from the posterior distribution, a constant z_0 was also used in the first tests. However, the resulting acoustic impedance realizations contained vertical "stripes" that might conceal the lateral structure. The problem seemed to be that some traces were much darker or brighter than they should have been, possibly due to very high or low reflection coefficients at the top of the trace. The following ad hoc modification was tested:

1. Calculate Z from C with constant z_0.
2. Calculate average acoustic impedance for each trace
$$\bar{Z}(x_i) = \frac{1}{n}\sum_{i=1}^{n} Z(x_i, t_j) \tag{6}$$
where n is the vertical grid size.
3. Calculate rescaled traces by
$$\tilde{Z}(x_i, t_j) = \frac{Z(x_i, t_j)}{\bar{Z}(x_i)}\tilde{Z}_0 \tag{7}$$

where $\tilde{Z}_0$ is a smooth function that makes the resulting $\tilde{Z}$ interpolate the well observations. (In the present case, with only two wells, $\tilde{Z}_0$ is linear). This procedure is used in the realizations from the posterior distribution shown in Section 4.

2.4 Simulations from the prior model

The model parameters used for simulations of acoustic impedance and reflection coefficients are summarized in Table 1 and 2. Some realizations from the prior distribution of Z using these parameters are shown in Figure 19. These realizations reflect the variability in the prior model. The vertical correlation structure has been selected based on well data. However it is hard to decide a horizontal correlation structure from the wells. The horizontal range has been set to 100 in these realizations to obtain some lateral continuity. For comparison, some realizations with horizontal range 20 are shown in Figure 20.

Z parameter		Value
exponential variogram parameters	horizontal range	100
	vertical range	15
	order ν	1.4

Table 1: Model parameters for acoustic impedance

C parameter	Value
Reflection coefficients expectation value	0
Reflection coefficients variance σ_C^2	0.035^2
Variogram	see Eq. 4 and parameters from Z variogram

Table 2: Model parameters for reflection coefficients

Φ parameter		Value
μ_Φ	$b_1 - b_2 z$	see Section 2.1
σ_Φ		see Section 2.1
exponential variogram parameters	horizontal range	26.7
	vertical range	4
	order ν	1.2

Table 3: Model parameters for porosity

3 Observations and likelihood model

The reservoir specific observations in this case are well data and seismic data. The realizations from the posterior distribution should honor these observations within the error bounds specified in the model. The well data are assumed to be exact. The model specified in Eide et al. (1997) requires that the well observations of acoustic impedance should be exact. It is not required that the well observations of porosity are exact, but it is assumed here for simplicity. The seismic data are assumed to be linearly related to the reflection coefficients. In Eide et al. (1997), the linear forward model is written

$$D = AC + U_D \tag{8}$$

where D is a vector containing seismic data, C is a vector of reflection coefficients, A is a known matrix defined by the seismic pulse and U_D is a Gaussian vector with zero mean and covariance matrix Σ_D.

3.1 The seismic wavelet

A 40 Hz Ricker wavelet, Figure 6, is used in the seismic forward model. This pulse was decided on by the geophysicists providing the data, and it was not considered to be important to do any pulse estimation.

3.2 Seismic noise

The linear seismic forward model in equation 8 assumes that the seismic noise U_D is Gaussian with zero mean and covariance matrix Σ_D. This error term includes both modeling error and measurement error. The modeling error includes all events not described by the linear forward model, for example multiple reflections.

In the synthetic example in Eide et al. (1997) it is assumed that U_D is white noise, that is, Σ_D is diagonal. However in the case where U_D contains events not included in the simple linear model, it is likely that the difference between the model and the observed seismic waveform will have the shape of a seismic pulse. This means that the errors that are close in time on the seismic trace will be correlated since the pulse length is larger than the vertical grid resolution. Hence other model types for the seismic observations error could be more realistic, but I keep the simplest model for computational reasons.

In the simplest form, where U_D is white noise, the correlation matrix Σ_D can be written $\sigma_D^2 I$ where I is the identity matrix. The noise variance σ_D^2 remains to be estimated.

Consider a single datum $d_{ij} = D(x_i, t_j)$ on a seismic trace. Under the linear model it is a weighted sum of reflection coefficients plus a noise term u_D, that is

$$d_{ij} = a^T c + u_D \tag{9}$$

where the vector a contains $2l+1$ weights determined by the seismic pulse and c is a vector of reflection coefficients at position (x_i, t_k), $k = j-l, \ldots, j+l$. Then the noise variance $\sigma_D^2 = \mathrm{var}(u_D)$ can be determined from the correlation between observed and modeled seismic data, if the the weights a and the correlation structure of c is known:

$$\sigma_D^2 = \sigma_M^2 \left(\frac{1}{\mathrm{corr}(d, a^T c)^2} - 1 \right). \tag{10}$$

Here σ_M^2 is the variance of the weighted sum $a^T c$. It may be easier in a practical situation to relate to correlation between the observed data and the model, than to the numerical value of the seismic noise variance.

3.3 Likelihood parameters

The model parameters used in the seismic forward model are given in Table 4.

D parameter	Value
Seismic pulse peak frequency	40 Hz
Seismic amplitude scaling κ	17857
Seismic noise variance σ_D^2	0.14^2 (correlation 0.99)

Table 4: Model parameters for the seismic forward model

4 Posterior model

Using the model specified above, simulations from the posterior distribution conditioned to seismic and well data were performed. A set of porosity and acoustic impedance realizations are shown in Figure 21 and 22 respectively.

To generate these realizations, reflection coefficients were simulated from the posterior distribution of C conditioned to reflection coefficients well data and observed seismic data. Then acoustic impedance realizations were calculated from the simulated reflection coefficients, with starting value z_0 calculated as specified in Section 2.3.

As mentioned in Section 1.4, the correlation between synthetic seismic traces calculated from well data, and the observed seismic traces at the wells, is low. This is also visible in the realizations in Figure 22, where the impedance in traces near the well at trace 143 stands out from the rest. In these simulation the parameters used in the likelihood function of the seismic data are fixed at the values given in Table 4.

Using the linear relation (1), $\mu(z)$ is calculated from the acoustic impedance realizations. Addition of U_Φ and conditioning on ϕ^o gives the porosity realizations shown in Figure 21.

The realizations from the posterior distribution should reproduce seismic data up to the precision of the observations. In Figure 23, seismic responses calculated from the three first realizations in Figure 22 are compared to the observed seismic data. The synthetic seismics from the three realizations reproduce the main features of the observed seismic data. The synthetic realizations are smoother than the observed data because the modeling and observational error is not reproduced. The residuals are shown in Figure 24. The residuals are large near the wells due to the misfit between seismic data and well data.

In Figure 25, histograms of porosity and acoustic impedance values in one realization from the posterior distribution are shown. In opposition to the well data histograms in Figure 10 and 11, these are clearly unimodal. Both histograms have a shape that resembles a Gaussian distribution, but they are skewed. This can be explained by the model, where reflection coefficients are Gaussian, and acoustic impedances are a transformation of these. Porosity is modeled as a sum of a non-Gaussian trend and a Gaussian residual.

In Figure 26, porosity in the wells are compared to porosity in traces away from the wells in a realization from the posterior distribution. A similar comparison for acoustic impedance is shown in Figure 27. The model specifications are such that the well data are exactly reproduced in realizations from the posterior distribution. These plots give an impression of the vertical correlation structure in the realizations, compared to the wells. The most striking difference is the "spikes" in acoustic impedance in the well at trace 47. Nothing similar to this appears in the traces away from the wells. The spikes may be due to thin, high impedance calcite sheets. The thickness of the calcite sheets is below seismic resolution and they are not easily reproduced by the Gaussian model used here.

5 Discussion and conclusions

A stochastic model for porosity and acoustic impedance conditioned to seismic data and well data has been applied to real data. The model is partly Gaussian, which makes it computationally attractive. These model assumptions are not in conflict with the data, as it was shown in Section 2. The model makes it possible to generate a large number of realizations that agree with seismic data and well data.

However, the Gaussian model is not good for reproducing thin high impedance layers due to calcites. Proper modeling of the calcites calls for other types of models; one possibility is marked point models. A possible extension of the model is to combine a marked point model for calcites with a Gaussian model for the sandstone background.

In this case study, wells and seismic data gave conflicting information in the region under study. This problem has not been fully solved here. Part of the solution might be in time/depth conversion or in connecting the well location to a particular seismic trace. This is outside the scope of this report.

5.1 Computing time

The computer program for simulation of Gaussian random fields conditionally on seismic data is based on sequential simulation and local conditioning similar to Omre, Sølna & Tjelmeland (1993). Since the amount of seismic data gives a large number of conditioning data points, the set of local conditioning points will be quite large. The most computer intensive part of the simulation is selection of conditioning points and calculation of weights. When this has been done, hundreds of realizations can be generated within a few seconds.

Selection of conditioning points and calculation of weights for simulation of the field of reflection coefficients, conditioned on seismic data and well data, takes approximately 9 hours.

Selection of conditioning points and calculation of weights for simulation of U_Φ conditioned on porosity well data takes approximately 16 minutes.

By using a partly Gaussian model, it is possible to sample the model directly. Iterative techniques may take considerably longer time due to the low acceptance probabilities, see Abrahamsen, Buland, Bølviken, Hauge, Hektoen & Skorstad (1996) for a more detailed discussion.

Acknowledgments

I thank the Troll unit members for the permission to publish this paper, Norsk Hydro ASA for providing the data, and Gyrid Johnsen and Åshild Skålnes at Norsk Hydro ASA for help, comments and enthusiastic discussions. The research is funded by a research grant from the Research Council of Norway.

References

Abrahamsen, P., Buland, A., Bølviken, E., Hauge, R., Hektoen, A. & Skorstad, A. (1996), Conditioning stochastic reservoir models on seismic amplitude traces — Stochastic inversion and simulation, NR-note SAND/07/1996, Norwegian Computing Center, P.O.Box 114 Blindern, N-0314 Oslo, Norway.

Eide, A. L., Ursin, B. & Omre, H. (1997), Stochastic simulation of porosity and acoustic impedance conditioned to seismic data and well data, *in* '67th Annual Meeting of the Society of Exploration Geophysicists, Expanded Abstracts', SEG, Dallas, Texas.

Omre, H., Sølna, K. & Tjelmeland, H. (1993), Simulation of random functions on large lattices, *in* A. Soares, ed., 'Geostatistics Tróia '92', proc. '4th Inter. Geostat. Congr.', Tróia Portugal, 1992, Kluwer Academic Publishers, Dordrecht, pp. 179–199.

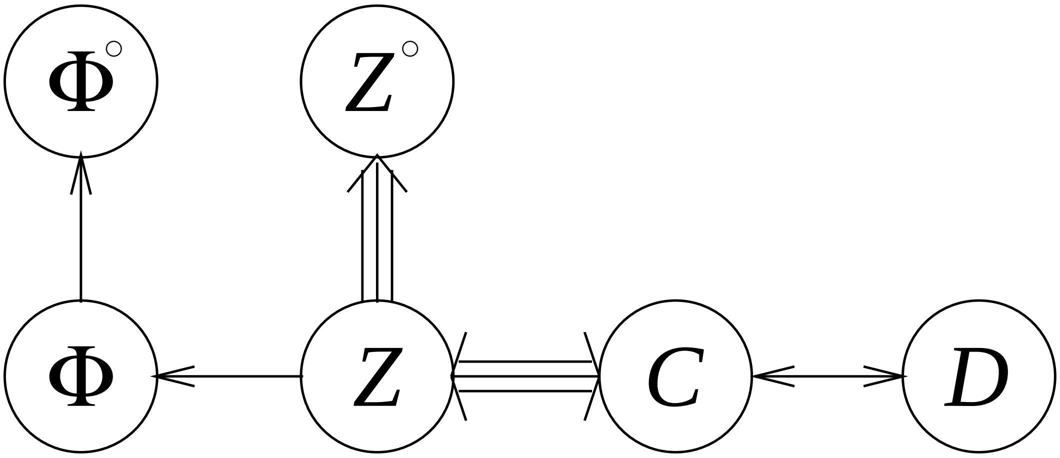

Figure 1: Graphical model showing relations between variables involved in the reservoir model. Seismic data D and reflection coefficients C have a bi-Gaussian distribution. Between C and the acoustic impedance Z there is a deterministic relation. Porosity Φ is Gaussian given Z. Well observations of acoustic impedance, Z^o, are a subset of Z. Well observations of porosity, Φ^o, can be any linear function of Φ.

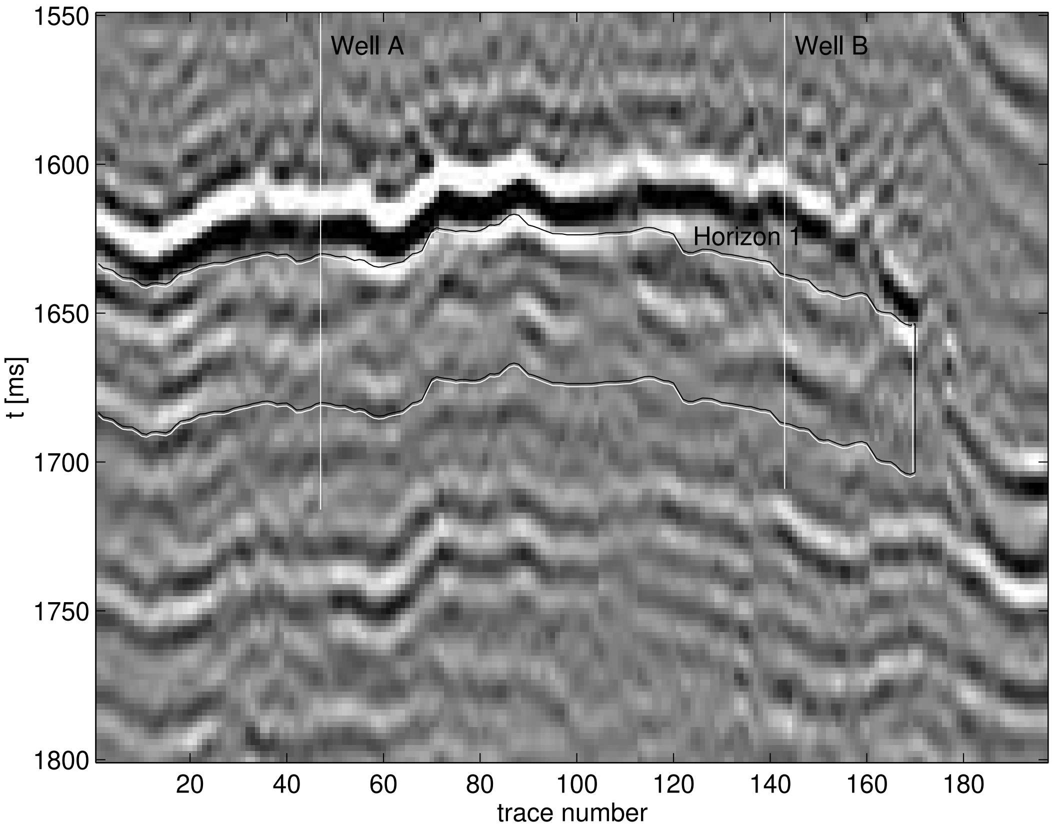

Figure 2: Seismic section with wells. The 50 ms window studied here is outlined.

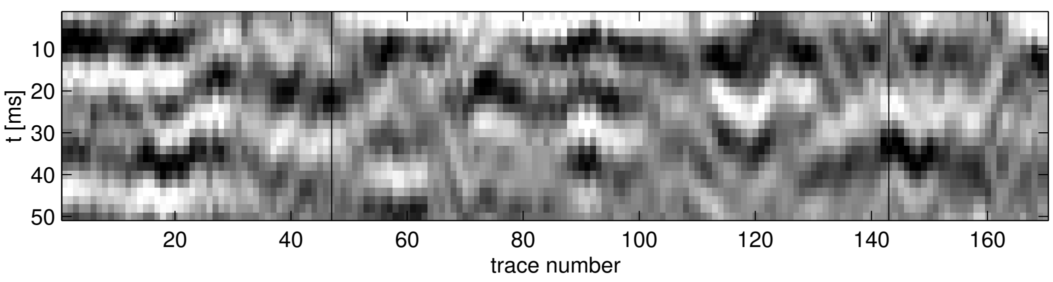

Figure 3: Window of 50 ms from seismic section, flattened relatively to horizon 1.

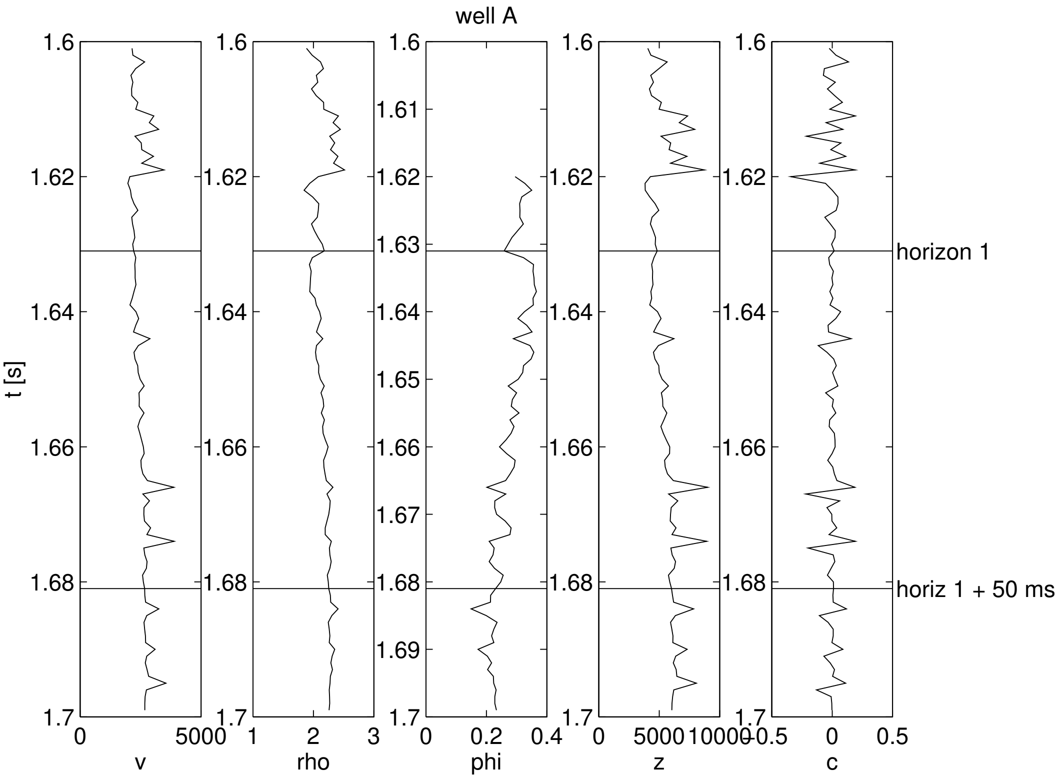

Figure 4: Well A. From left to right: velocity (v), density (ρ), porosity (ϕ), impedance (z) and reflection coefficients (c).

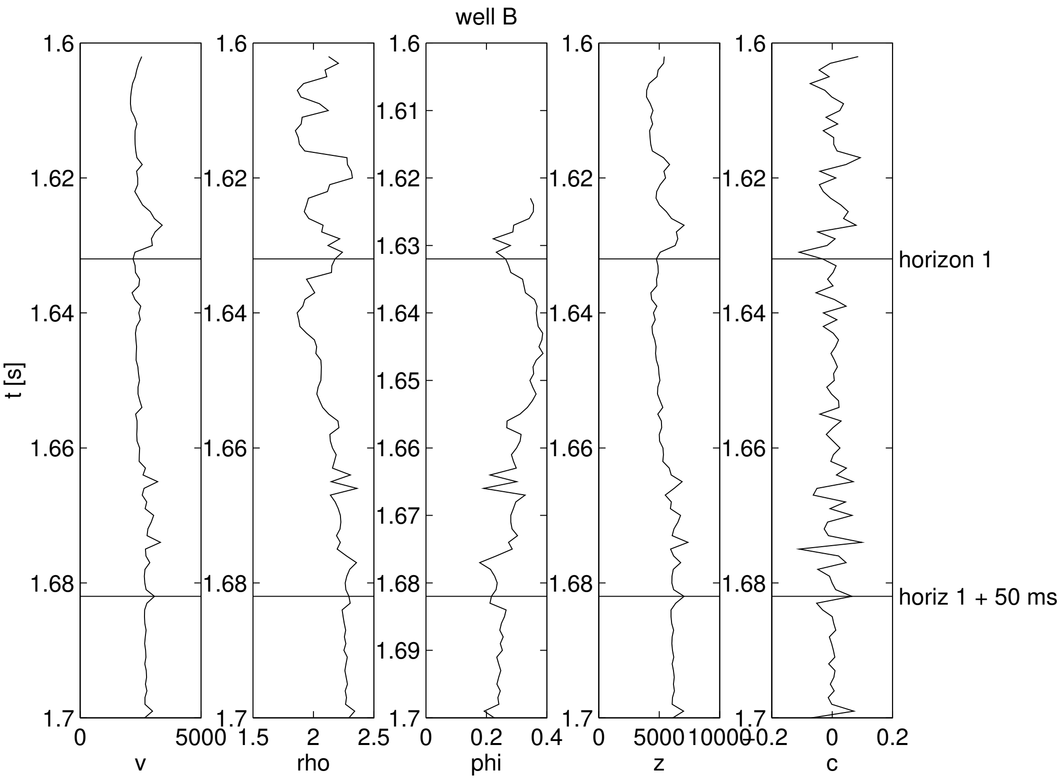

Figure 5: Well B. From left to right: velocity (v), density (ρ), porosity (ϕ), impedance (z) and reflection coefficients (c)

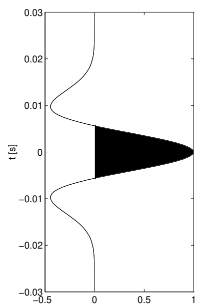

Figure 6: 40 Hz Ricker wavelet used for seismic reflection modeling. The pulse that is used in the modeling has the opposite polarity of what is shown in the figure.

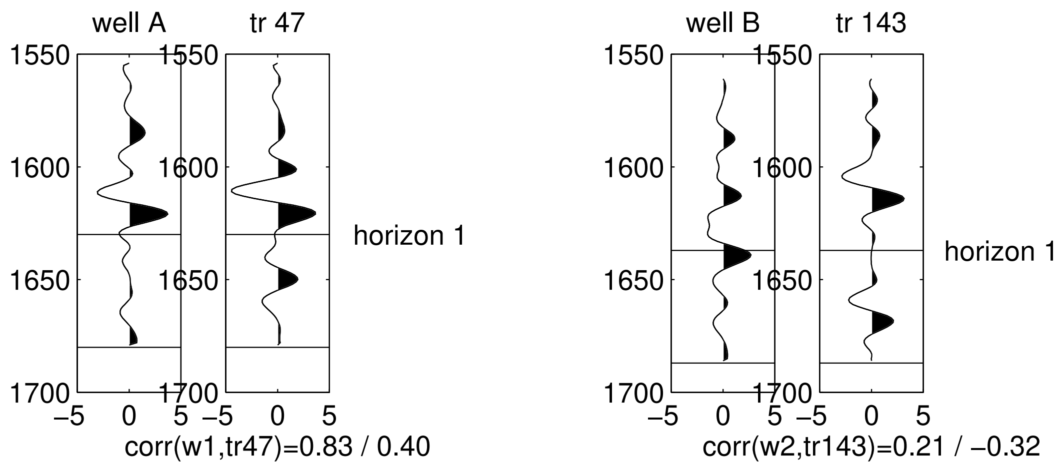

Figure 7: Synthetic and observed seismic traces at wells. Horizontal lines indicate the 50 ms corresponding to the region under study.

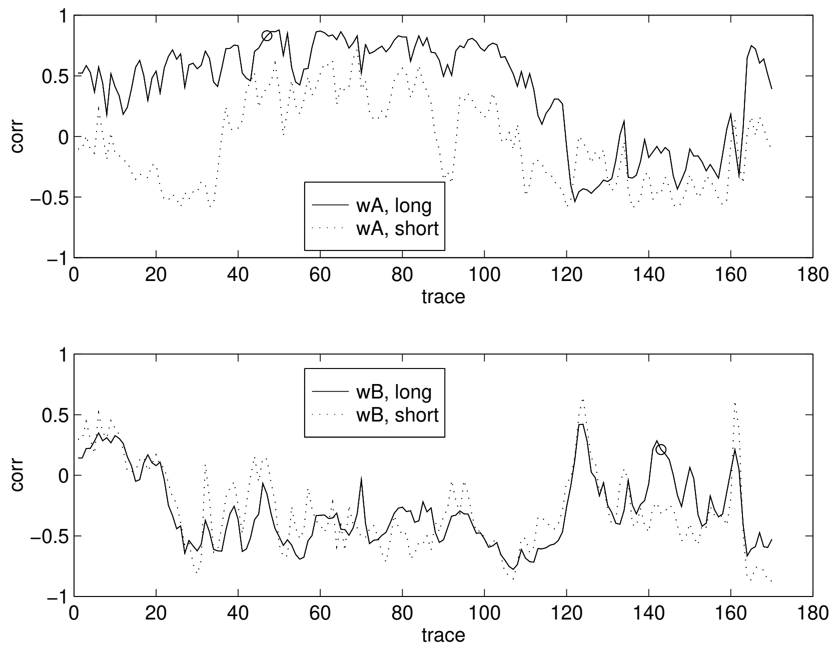

Figure 8: Correlation between the synthetic traces from the well data and all the observed traces, using the 126 ms window shown in Figure 7. Dotted lines show the correlations when using only the 50 ms window under study. Circles show the location of wells.

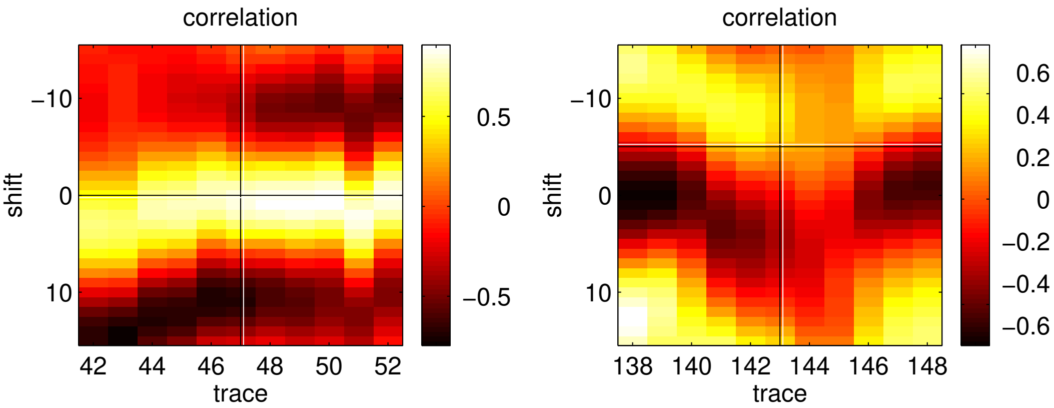

Figure 9: Correlation between the synthetic traces from the well data and the 5 closest observed traces, using the 126 ms window shown in Figure 7. The synthetic trace has been shifted ± 15 ms and correlation has been calculated for each 1 ms shift increment. The vertical and horizontal lines indicate the wells and shifts used in this case study.

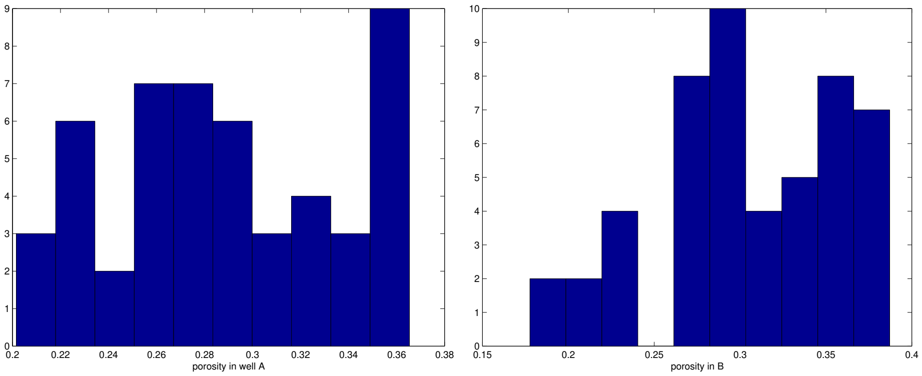

Figure 10: Histograms of porosity from well data

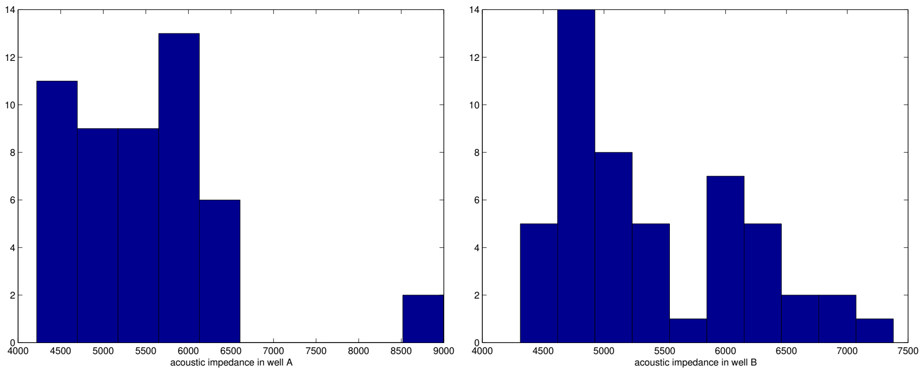

Figure 11: Histograms of acoustic impedance from well data

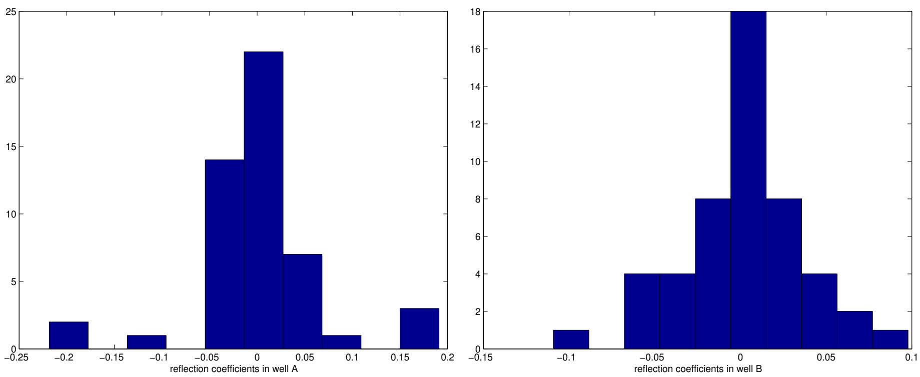

Figure 12: Histograms of reflection coefficients from well data

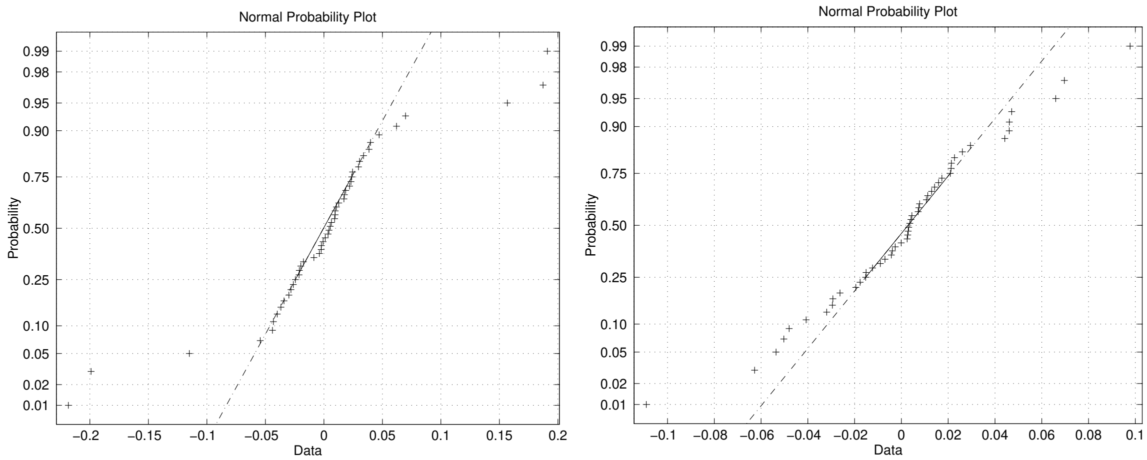

Figure 13: Normal probability plots of reflection coefficients from data from well A (left) and B (right). The 50 samples used are taken from the region below horizon 1. Most of the data points lie on a straight line, as they would do if the data came from a Gaussian distributions. The deviations from the straight line at the ends may indicate that the tails of the distributions are more heavy than for a normal distribution.

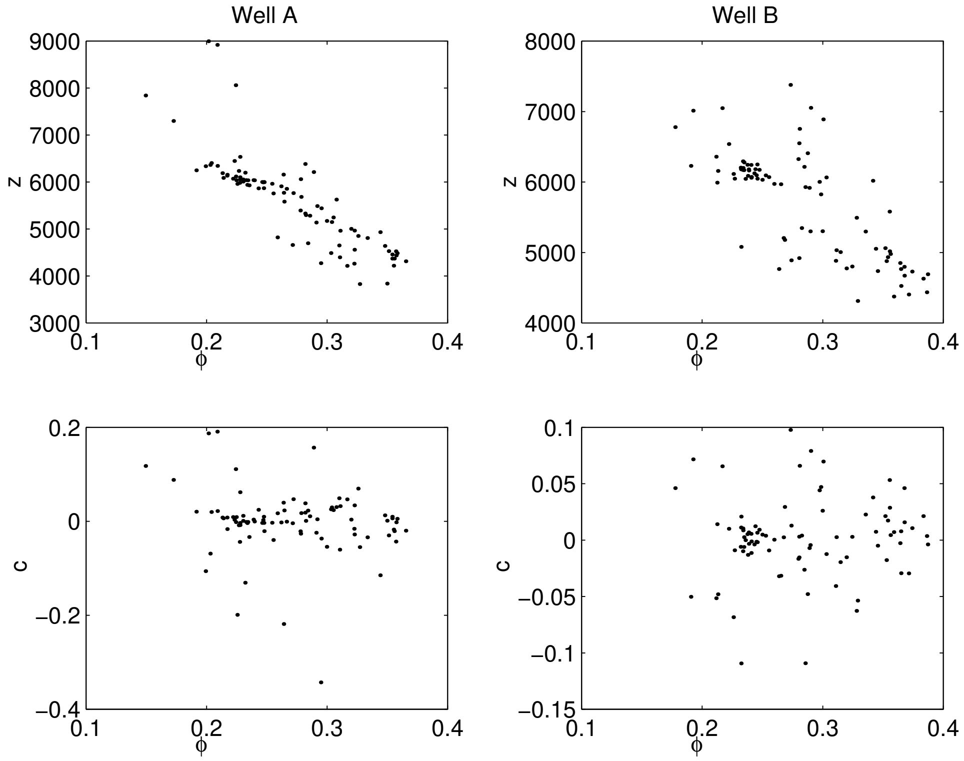

Figure 14: Cross plots of acoustic impedance (z) and porosity (ϕ) from well logs from well A (upper left) and well B (upper right) and cross plots of reflection coefficients (c) and porosity from well A (lower left) and well B (lower right).

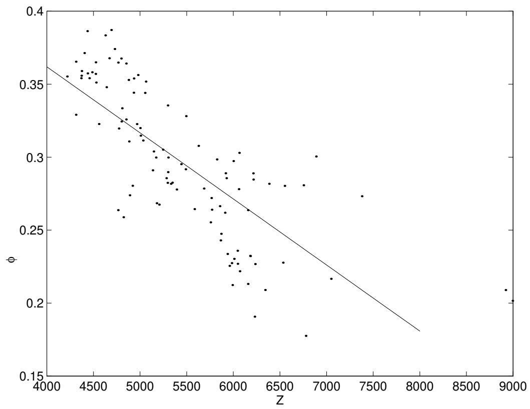

Figure 15: Porosity and acoustic impedance observations with regression line

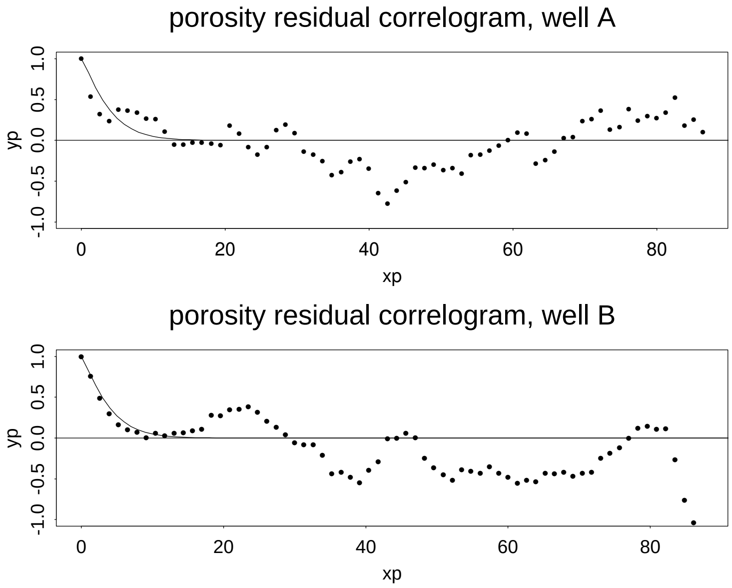

Figure 16: Correlation function for porosity residuals U_ϕ, fitted to empirical correlation from well data.

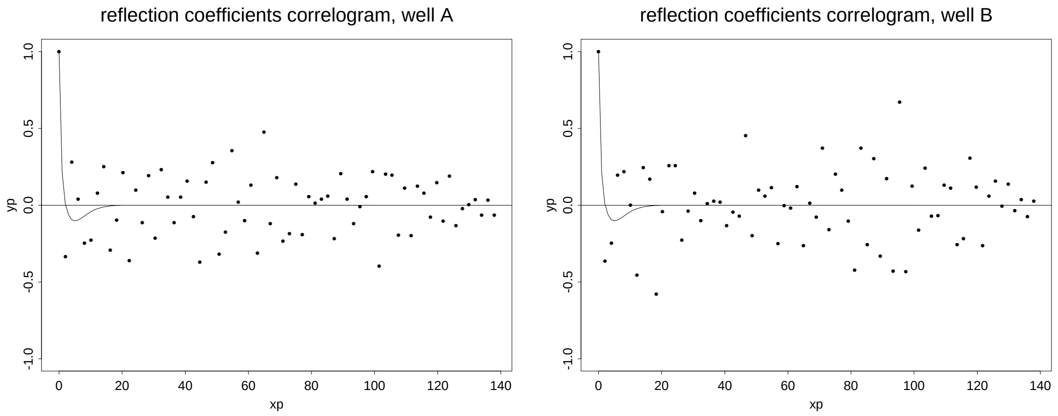

Figure 17: Correlation function for reflection coefficients, fitted to empirical correlation from well data

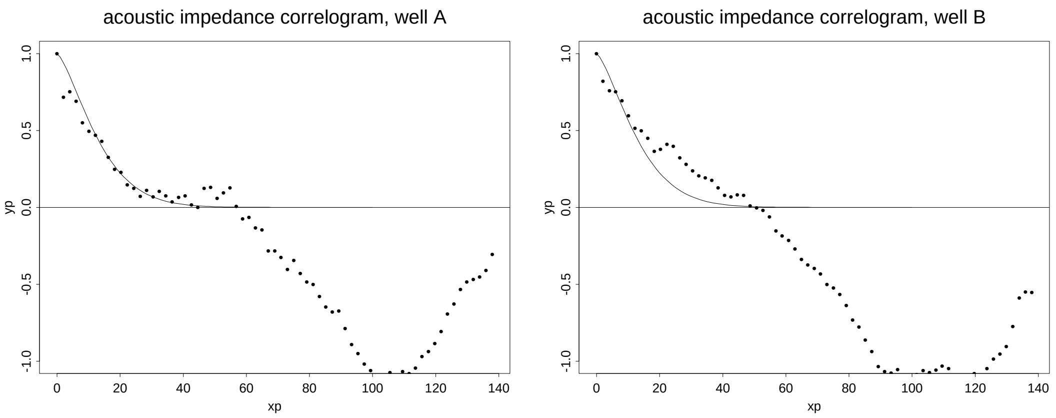

Figure 18: Correlation function for acoustic impedance, fitted to empirical correlation from well data

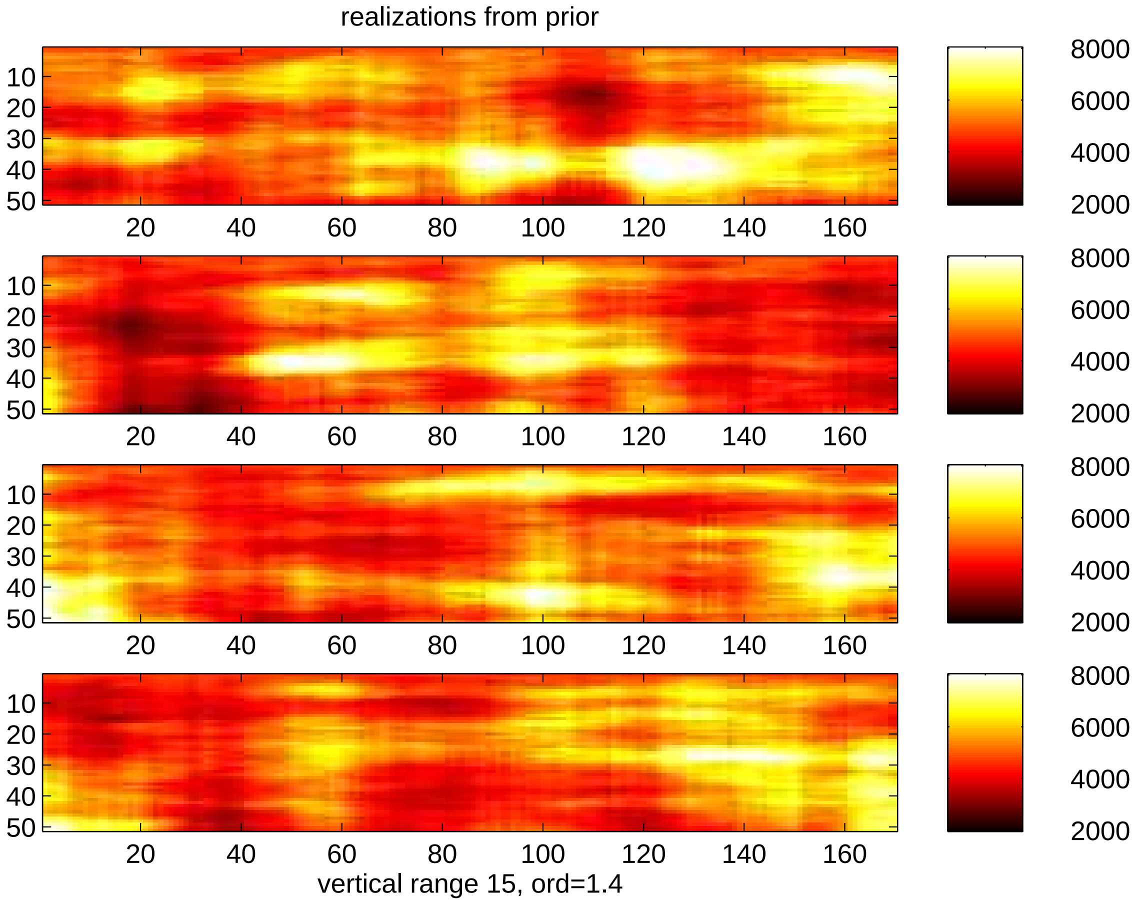

Figure 19: Realizations acoustic impedance from the prior model with parameters as specified in Table 1 and 2.

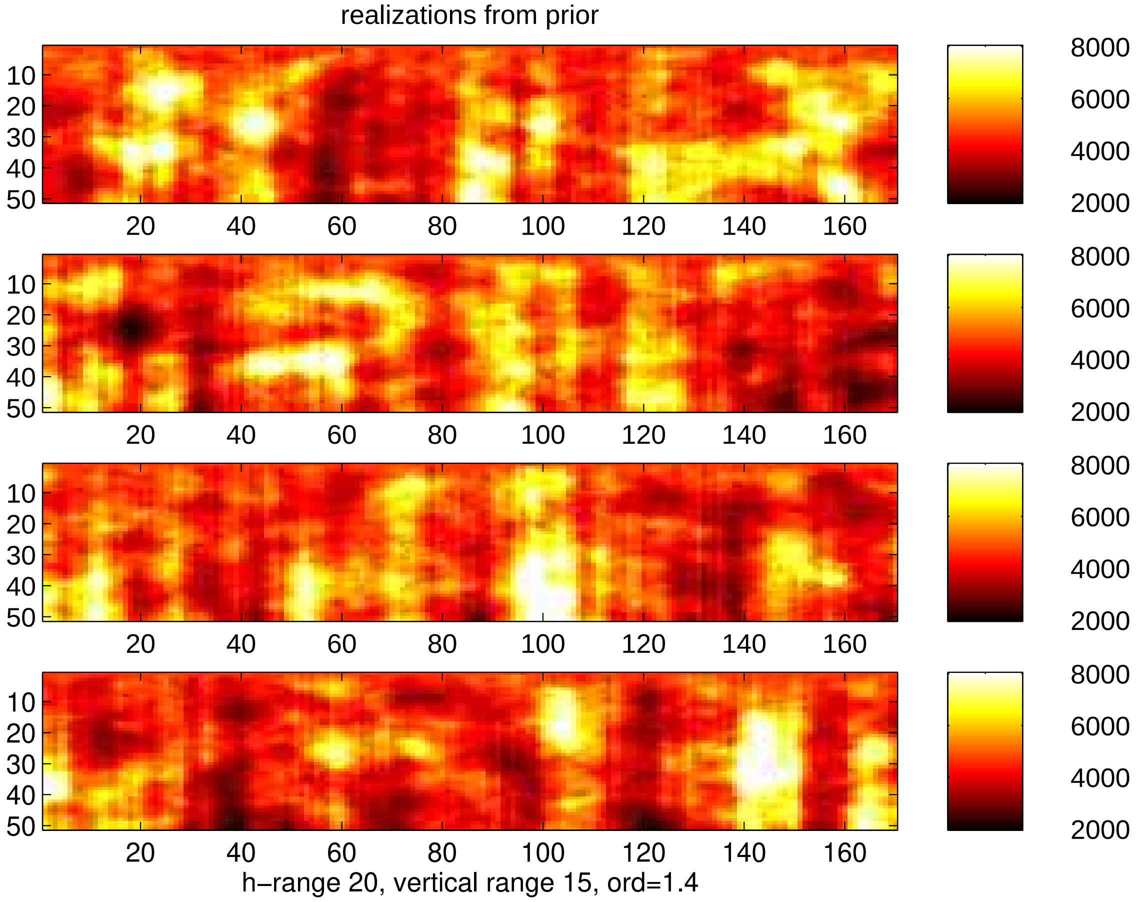

Figure 20: Realizations of acoustic impedance from prior model with parameters as in Figure 19, except that horizontal range has been reduced to 20.

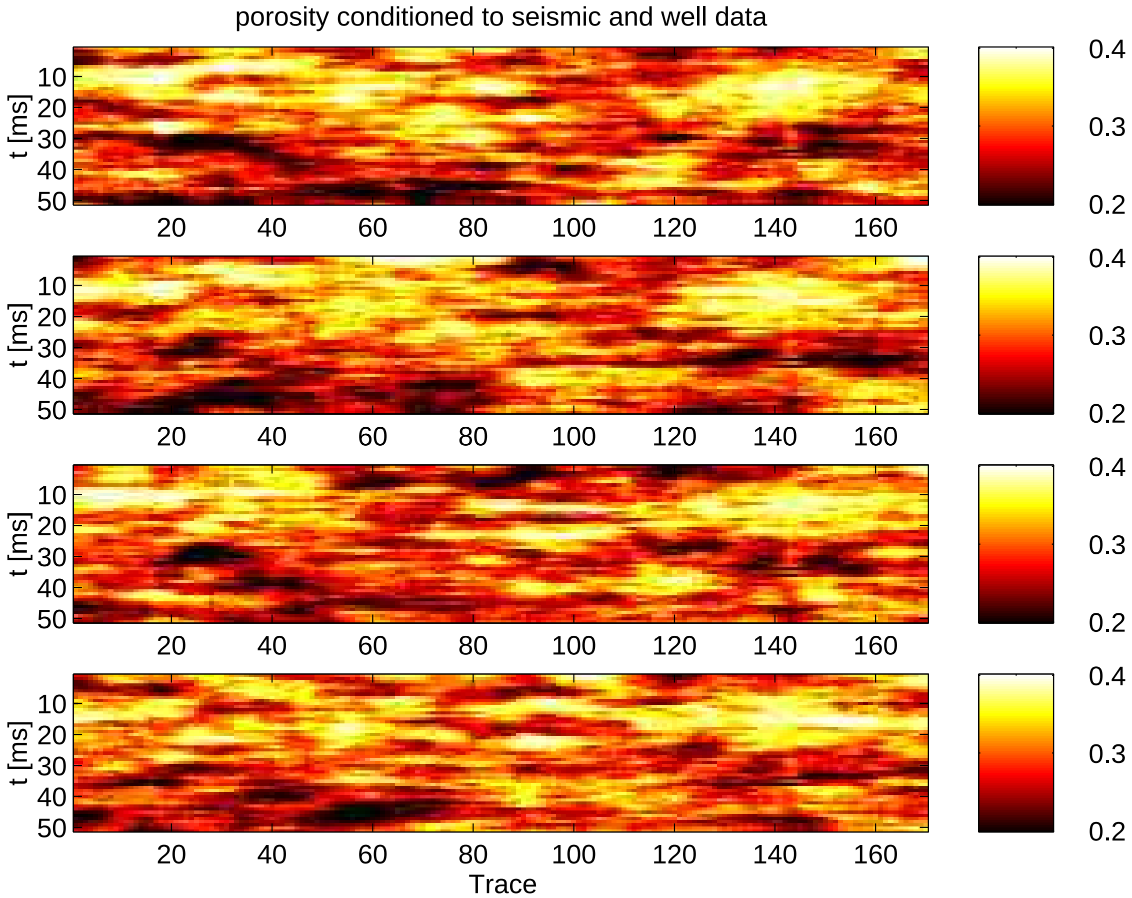

Figure 21: Four realizations from the posterior distribution of porosity conditioned to seismic data and well data

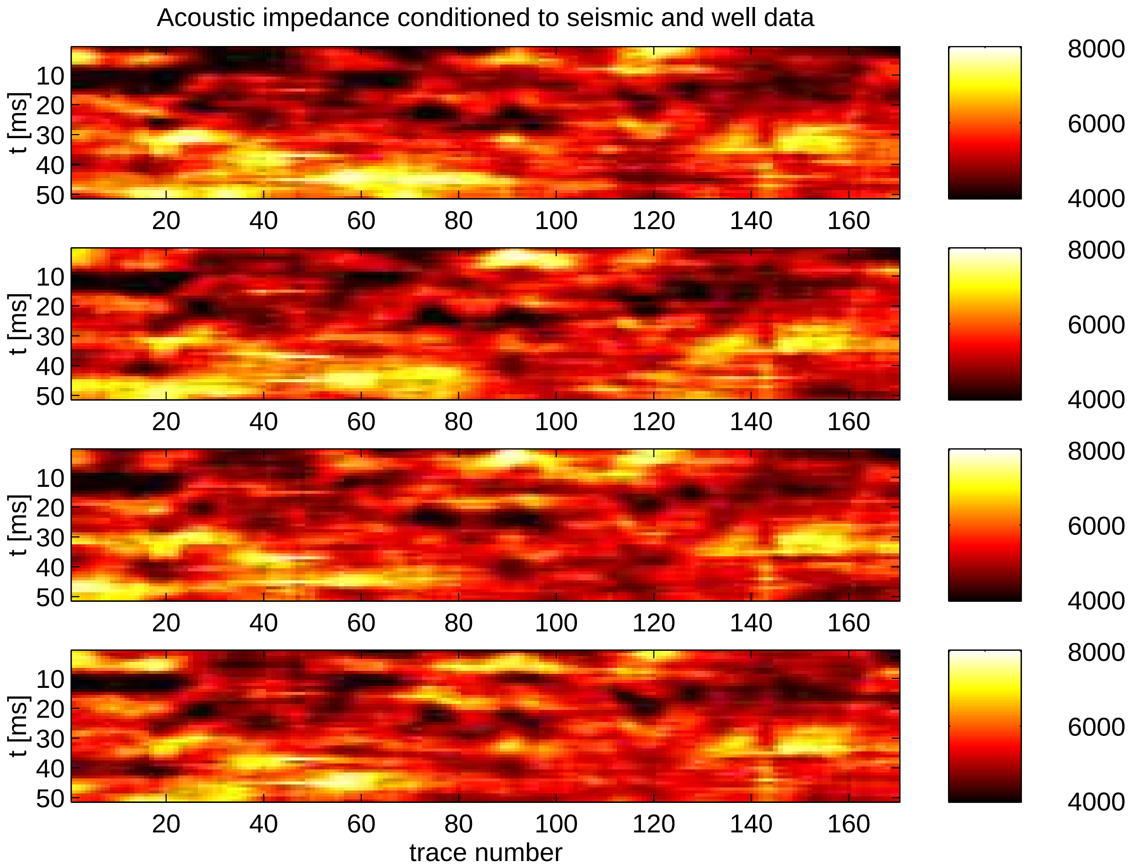

Figure 22: Four realizations from the posterior distribution of acoustic impedance conditioned to seismic data and well data

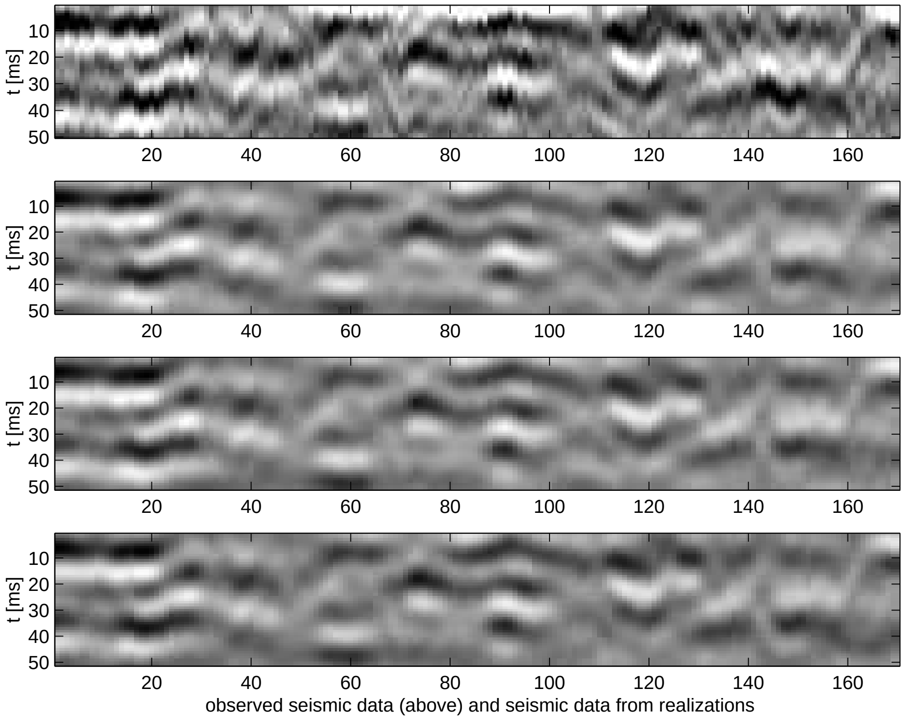

Figure 23: The observed seismic data, compared to seismic data from 3 realizations from the posterior distribution of acoustic impedance conditioned to seismic data and well data.

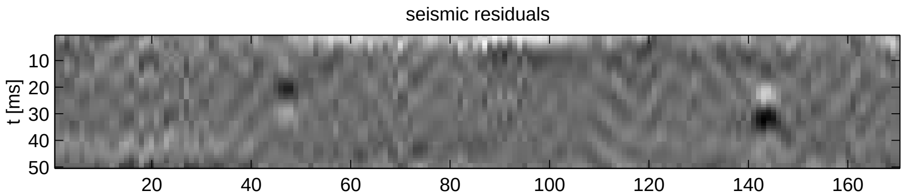

Figure 24: Seismic residuals; the difference between the observed seismic data and seismic data from a realization from the posterior distribution.

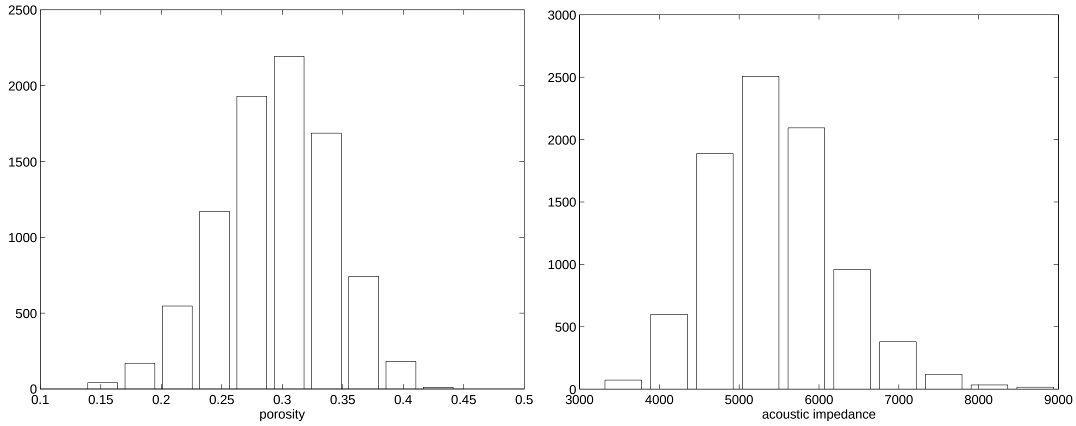

Figure 25: Histograms of porosity and acoustic impedance in one of realizations from the posterior distribution

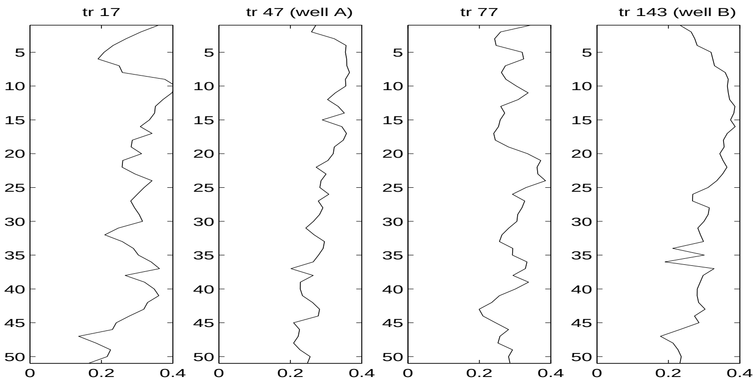

Figure 26: Comparison of porosity well data and porosity along two traces in a realization from the posterior distribution. Number 2 and 4 from the left are well data, the other two are traces away from the wells.

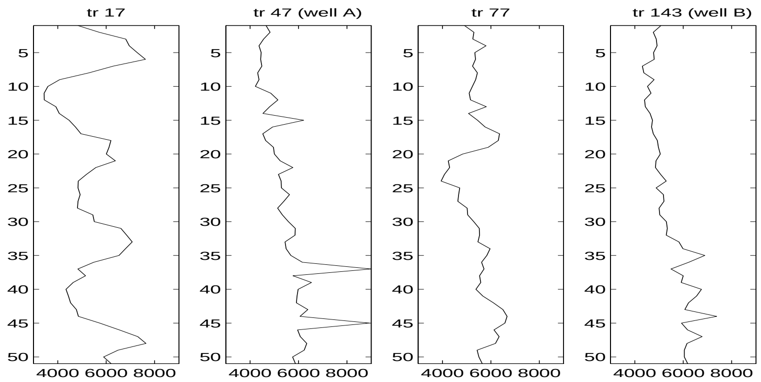

Figure 27: Comparison of acoustic impedance well data and acoustic impedance along two traces in a realization from the posterior distribution. Number 2 and 4 from the left are well data, the other two are traces away from the wells.